

Variational quantum algorithm for generalized eigenvalue problems of non-Hermitian systems

Jiaxin Li,¹ Zhaobing Fan,¹ Hongmei Yao,^{1,*} Chunlin Yang,¹ Shao-Ming Fei,^{2,†} Zi-Tong Zhou,³ and Teng-Yang Ma³

¹*School of Mathematical Sciences, Harbin Engineering University, Harbin 150001, China*

²*School of Mathematical Sciences, Capital Normal University, Beijing 100048, China*

³*Origin Quantum Computing Technology Co., Ltd., Hefei 230088, China*

(Dated: July 8, 2025)

Most quantum algorithms for generalized eigenvalue problems focus on Hermitian systems, and few are applicable to non-Hermitian systems. Based on the generalized Schur decomposition, we propose a variational quantum algorithm for solving generalized eigenvalue problems in non-Hermitian systems. The algorithm transforms the generalized eigenvalue problem into a process of searching for unitary transformation matrices. Moreover, we develop a method for evaluating both the loss function and its gradients on near-term quantum devices. Finally, we numerically validate the algorithm's performance through simulations and demonstrate its application to generalized eigenvalue problems in ocean acoustics. The algorithm's robustness is further confirmed through noise simulations.

I. INTRODUCTION

Generalized eigenvalue problems hold fundamental importance across mathematics and applied science, and its theoretical and applied value has been widely recognized in many disciplines. In the past 100 years, people have never stopped the study of solving generalized eigenvalue problems. Various methods have been developed for solving generalized eigenvalue problems in classical computation [1–3]. A key issue is that memory usage and computational complexity explode as the system scales, making it challenging for classical computers to solve large-scale generalized eigenvalue problems [4].

The rapid development of quantum computing technology provides a solution to this challenge [5–8]. As a highly promising approach for high-performance computing, quantum computing offers significant speed advantages over classical computing due to its capability to handle exponentially large Hilbert spaces. The quantum phase estimation (QPE) algorithm, originally developed to calculate molecular ground-state energies in quantum chemistry [9, 10], has been extended in fault-tolerant quantum computers to solve generalized eigenvalue problems [11, 12]. Meanwhile, the variational quantum eigensolver (VQE)—a classical-quantum hybrid framework designed to estimate ground state energies of Hamiltonians on near-term quantum devices [13–15]—has been further extended to the variational quantum generalized eigensolver (VQGE) for computing minimal generalized eigenvalues of Hamiltonians [16–18]. Both VQE and VQGE belong to the family of variational quantum algorithm (VQA) [19], which minimize or maximize the expectation value of observables through parameterized a quantum circuits (PQC) or simply an ansatz. VQA have been widely applied to diverse problems and have emerged as

a leading approach for achieving quantum advantage in the near term [20–23]. However, existing quantum algorithms are only applicable to generalized eigenvalue problems in Hermitian systems, and cannot be directly extended to non-Hermitian systems. Currently, quantum algorithms capable of evaluating generalized eigenvalues in non-Hermitian systems remain scarce. Given the broad applications of non-Hermitian generalized eigenvalue problems in ocean acoustics, mechanical engineering, and related fields, developing quantum algorithms specifically for non-Hermitian systems carries substantial theoretical and practical importance.

In this paper, we present a variational quantum generalized eigensolver (VQGE) for solving the generalized eigenvalue problem in non-Hermitian systems. The remainder of this paper is organized as follows. Section II establishes the theoretical framework of VQGE and defines the loss function. Section III elaborates the method for computing the loss function and its gradients on near-term quantum devices. Section IV details the VQGE algorithm. Section V presents the complexity analysis. Section VI conducts numerical simulations with applications to ocean acoustics problems. Finally, we draw conclusions in Section VII.

II. THEORETICAL FRAMEWORK AND LOSS FUNCTION

Consider two matrices $A, B \in \mathbb{C}^{N \times N}$, the generalized eigenvalue equation is expressed as

$$A|\psi\rangle = \lambda B|\psi\rangle. \quad (1)$$

where λ is the generalized eigenvalue of matrix pair (A, B) , and $|\psi\rangle$ is the corresponding eigenvector.

To determine the generalized eigenvalues of (A, B) , our variational quantum generalized eigensolver employs the generalized Schur decomposition theory [24]. The theory states that for any $A, B \in \mathbb{C}^{N \times N}$ there exist unitary

* hongmeiyao@163.com

† feishm@cnu.edu.cn

matrices Q and Z such that

$$Q^\dagger AZ = T, \quad Q^\dagger BZ = S, \quad (2)$$

where T and S are upper triangular matrices. Let $\lambda(A, B)$ denote the set of generalized eigenvalues of the matrix pair (A, B) . If for some k , t_{kk} and s_{kk} are both zero, then $\lambda(A, B) = \mathbb{C}$. Otherwise

$$\lambda(A, B) = \left\{ \frac{t_{ii}}{s_{ii}} \mid s_{ii} \neq 0 \right\}.$$

Based on the Schur decomposition theory, for given matrices $A, B \in \mathbb{C}^{2^n \times 2^n}$, we define the loss function as

$$\begin{aligned} \mathcal{L}(\boldsymbol{\theta}, \boldsymbol{\phi}) &= \sum_{i=1}^{2^n-1} \sum_{j=0}^{i-1} (|\langle i | Q^\dagger(\boldsymbol{\theta}) AZ(\boldsymbol{\phi}) | j \rangle|^2 \\ &\quad + |\langle i | Q^\dagger(\boldsymbol{\theta}) BZ(\boldsymbol{\phi}) | j \rangle|^2) \\ &= \sum_{i=1}^{2^n-1} \sum_{j=0}^{i-1} (|\langle i | T(\boldsymbol{\theta}, \boldsymbol{\phi}) | j \rangle|^2 + |\langle i | S(\boldsymbol{\theta}, \boldsymbol{\phi}) | j \rangle|^2) \end{aligned} \quad (3)$$

where $T(\boldsymbol{\theta}, \boldsymbol{\phi}) = Q^\dagger(\boldsymbol{\theta})AZ(\boldsymbol{\phi})$, $S(\boldsymbol{\theta}, \boldsymbol{\phi}) = Q^\dagger(\boldsymbol{\theta})BZ(\boldsymbol{\phi})$, with $Q(\boldsymbol{\theta})$ and $Z(\boldsymbol{\phi})$ being parameterized unitary matrices, and $|i\rangle$ denotes the i -th computational basis state.

Theorem 1. The loss function $\mathcal{L}(\boldsymbol{\theta}, \boldsymbol{\phi})$ reaches its global minimum of zero if and only if $T(\boldsymbol{\theta}, \boldsymbol{\phi})$ and $S(\boldsymbol{\theta}, \boldsymbol{\phi})$ are upper triangular matrices.

Proof. (\Rightarrow) If $\mathcal{L}(\boldsymbol{\theta}, \boldsymbol{\phi}) = 0$, since all terms in (3) are non-negative sums, it follows that

$$|\langle i | T(\boldsymbol{\theta}, \boldsymbol{\phi}) | j \rangle|^2 = |\langle i | S(\boldsymbol{\theta}, \boldsymbol{\phi}) | j \rangle|^2 = 0$$

for all indices $i = 1, \dots, 2^n - 1, j = 0, \dots, i - 1$. This satisfies the definition of upper triangular matrices (all below-diagonal elements are zero).

(\Leftarrow) If $T(\boldsymbol{\theta}, \boldsymbol{\phi})$ and $S(\boldsymbol{\theta}, \boldsymbol{\phi})$ are upper triangular, then

$$|\langle i | T(\boldsymbol{\theta}, \boldsymbol{\phi}) | j \rangle|^2 = |\langle i | S(\boldsymbol{\theta}, \boldsymbol{\phi}) | j \rangle|^2 = 0$$

for all indices $i = 1, \dots, 2^n - 1, j = 0, \dots, i - 1$. Direct substitution into (3) yields $\mathcal{L}(\boldsymbol{\theta}, \boldsymbol{\phi}) = 0$.

Since \mathcal{L} is a sum of non-negative terms, zero is its global minimum. \square

For matrices A and B with dimensions smaller than $2^n \times 2^n$, they can be embedded into a $2^n \times 2^n$ dimensional space by constructing block matrices

$$\tilde{A} = \begin{pmatrix} A & 0 \\ 0 & I \end{pmatrix}, \quad \tilde{B} = \begin{pmatrix} B & 0 \\ 0 & I \end{pmatrix},$$

where I is the identity matrix. Under this construction, the generalized eigenvalues of \tilde{A} and \tilde{B} are identical to those of the original matrices A and B , except for the addition of trivial eigenvalues equal to 1, which do not affect the solution to the original problem. Thus, this work focuses exclusively on the case where A and B are $2^n \times 2^n$ matrices. In Section III, we present the estimation method of the loss function on near-term quantum devices.

III. THE COMPUTATION OF LOSS FUNCTION

Since the strictly lower triangular parts of matrices $T(\boldsymbol{\theta}, \boldsymbol{\phi})$ and $S(\boldsymbol{\theta}, \boldsymbol{\phi})$ contain $2^n(2^n - 1)$ elements, evaluating the loss function in (3) requires at least $O(2^{2n})$ measurements. Under these conditions, the quantum approach would have no advantage. Therefore, in computing the loss function, we employ the quantum process snapshot (QPS) technique from [14], which could measure elements from one matrix within a single quantum circuit. For convenience, we incorporating index register enables simultaneous measure elements from multiple matrices within a single quantum circuit (implementation details are provided in Appendix A). The loss function can be computed via the quantum circuit shown in Fig. 1, where $Q^\dagger(\boldsymbol{\theta})$ and $Z(\boldsymbol{\phi})$ are parameterized quantum circuits. When matrices A and B are non-unitary, they can be encoded into quantum systems through data-input models such as block encoding [25, 26] or linear combination of unitaries (LCU) [27, 28] et al. Unitary matrices U_A and U_B are employed to realize the quantum encoding of A and B respectively. In this work, we employ the LCU method as the foundational framework for quantum data input (quantum circuit in Appendix B). Without loss of generality, we decompose matrices A and B into linear combinations of 2^m unitary matrices. The registers follow this naming convention: $a(m)$ denotes ancilla register with m qubits, $w(n)$ denotes work register with n qubits, $\text{idx}(1)$ denotes index register with 1 qubit, and $\text{aug}(n)$ denotes augmented register with n qubits.

To implement matrices A and B on the augmented register, the measurement outcome of the ancilla register must be $|0\rangle^{\otimes m}$. When the state of ancilla register collapse to $|0\rangle^{\otimes m}$, the quantum circuit evolves the initial state $|0\rangle_w^{\otimes n} |0\rangle_a |0\rangle_{\text{aug}}^{\otimes n}$ into

$$\frac{1}{\sqrt{2^{n+1}}} \sum_{i=0}^{2^n-1} (|i\rangle_w |0\rangle_a T(\boldsymbol{\theta}, \boldsymbol{\phi}) |i\rangle_{\text{aug}} + |i\rangle_w |0\rangle_a S(\boldsymbol{\theta}, \boldsymbol{\phi}) |i\rangle_{\text{aug}}), \quad (4)$$

as discussed in Appendix C.

Theorem 2. Let N_L denote the number of measurement results in the set $L = \{|i\rangle_w |0\rangle_a |j\rangle_{\text{aug}}, |i\rangle_w |1\rangle_a |j\rangle_{\text{aug}} \mid i = 1, 2, \dots, N-1, j = 0, 1, \dots, i-1\}$, and N_{meas} represent the total number of measurements. The loss function is then computed as

$$\mathcal{L}(\boldsymbol{\theta}, \boldsymbol{\phi}) = 2^{n+1} \frac{N_L}{N_{\text{meas}}}. \quad (5)$$

Proof. The probability of observing a state $|i\rangle_w |k\rangle_a |j\rangle_{\text{aug}}$ is

$$P_{ijk} = \begin{cases} \frac{1}{2^{n+1}} |\langle i | T(\boldsymbol{\theta}, \boldsymbol{\phi}) | j \rangle|^2 & k = 0, \\ \frac{1}{2^{n+1}} |\langle i | S(\boldsymbol{\theta}, \boldsymbol{\phi}) | j \rangle|^2 & k = 1. \end{cases}$$

By summing these probabilities over all states in the

set L , we obtain the total probability

$$\begin{aligned} P_L &= \frac{1}{2^{n+1}} \sum_{i=1}^{2^n-1} \sum_{j=0}^{i-1} (|\langle i|T(\boldsymbol{\theta}, \boldsymbol{\phi})|j\rangle|^2 + |\langle i|S(\boldsymbol{\theta}, \boldsymbol{\phi})|j\rangle|^2) \\ &= \frac{1}{2^{n+1}} \mathcal{L}(\boldsymbol{\theta}, \boldsymbol{\phi}). \end{aligned}$$

Thus, through simple algebraic relations, we obtain

$$\mathcal{L}(\boldsymbol{\theta}, \boldsymbol{\phi}) = 2^{n+1} P_L = 2^{n+1} \frac{N_L}{N_{meas}}.$$

In practical implementations, the more measurements we do, the more accurate our answer becomes. \square

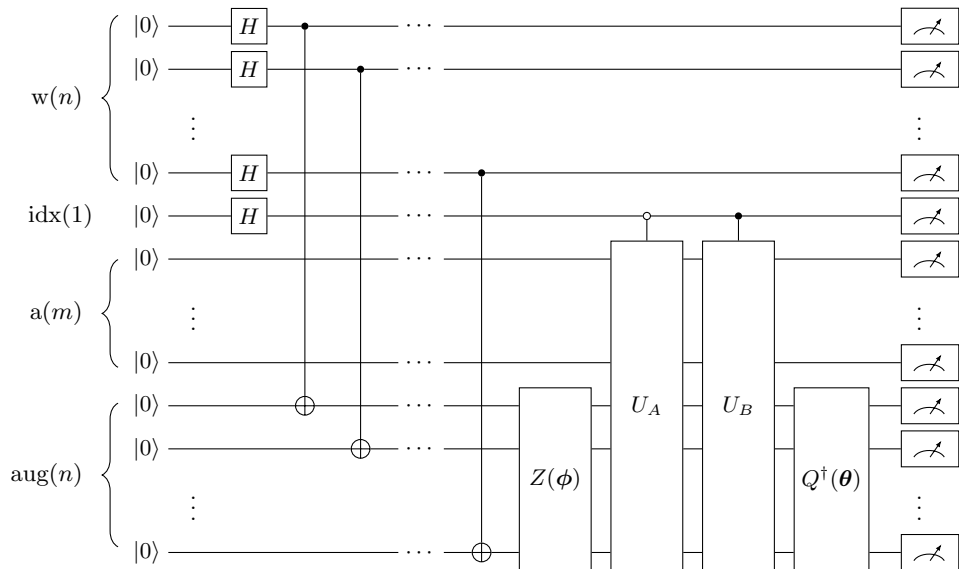


FIG. 1: Quantum circuit for computation of loss function in (3).

IV. VARIATIONAL QUANTUM GENERALIZED EIGENSOLVER

In our variational quantum generalized eigensolver, the inputs include the data input models U_A and U_B of matrices A and B , as well as the parameterized circuits $Q^\dagger(\boldsymbol{\theta})$ and $Z(\boldsymbol{\phi})$. After receiving the input, our algorithm enters a hybrid quantum-classical optimization loop. The parameterized quantum circuits $Q^\dagger(\boldsymbol{\theta})$ and $Z(\boldsymbol{\phi})$ are trained through the loss function $\mathcal{L}(\boldsymbol{\theta}, \boldsymbol{\phi})$, which can be calculated using equation (5). Then we feed back the value and gradient of the loss function to the classical computer, which updates the parameters $\boldsymbol{\theta}$ and $\boldsymbol{\phi}$ and proceeds to the next iteration. The objective is to find the optimal parameters $\boldsymbol{\theta}_{opt}$ and $\boldsymbol{\phi}_{opt}$ that globally minimize the loss function $\mathcal{L}(\boldsymbol{\theta}, \boldsymbol{\phi})$, which is

$$(\boldsymbol{\theta}_{opt}, \boldsymbol{\phi}_{opt}) = \arg \min_{\boldsymbol{\theta}, \boldsymbol{\phi}} \mathcal{L}(\boldsymbol{\theta}, \boldsymbol{\phi}).$$

It should be noted that while the quantum circuit is executed N_{meas} times, the matrices A and B are successfully implemented on the augmented qubits via U_A and U_B only when the measurement outcome of the ancilla register is $|0\rangle^{\otimes m}$. This introduces errors in computing both the loss function $\mathcal{L}(\boldsymbol{\theta}, \boldsymbol{\phi})$ and its gradient during gradient-based optimization. However, these errors can be mitigated by increasing the number of circuit executions to an appropriate level [29], as the probability of significant relative error decreases exponentially with the number of successful implementations. In practice, the optimal number of executions for achieving target precision should be determined empirically through repeated experiments. Accordingly, we perform measurements on all registers.

Algorithm 1 Variational quantum generalized eigensolver (VQGE)

- 1: **Input:** U_A , U_B , parameterized circuits $Q^\dagger(\boldsymbol{\theta})$ and $Z(\boldsymbol{\phi})$ with initial parameters of $\boldsymbol{\theta}_0$, $\boldsymbol{\phi}_0$, and error threshold ε ;
 - 2: Choose an appropriate number of circuit executions to compute the loss function $\mathcal{L}(\boldsymbol{\theta}, \boldsymbol{\phi})$;
 - 3: **while** $\mathcal{L}(\boldsymbol{\theta}, \boldsymbol{\phi})$ has not converged **do**
 - 4: $\theta_i \leftarrow \theta_i - \delta \frac{\partial \mathcal{L}}{\partial \theta_i}$;
 - 5: $\phi_i \leftarrow \phi_i - \delta \frac{\partial \mathcal{L}}{\partial \phi_i}$;
 - 6: **end while**
 - 7: **return** $\boldsymbol{\theta}_{opt}, \boldsymbol{\phi}_{opt}$;
 - 8: Let $T = Q^\dagger(\boldsymbol{\theta}_{opt})AZ(\boldsymbol{\phi}_{opt})$, $S = Q^\dagger(\boldsymbol{\theta}_{opt})BZ(\boldsymbol{\phi}_{opt})$;
 - 9: Obtain the diagonal elements $\{t_{ii}\}_{i=1}^N$ and $\{s_{ii}\}_{i=1}^N$ of matrices T and S using Hadamard test;
 - 10: Use the diagonal elements $\{t_{ii}\}_{i=1}^N$ and $\{s_{ii}\}_{i=1}^N$ to evaluate the generalized eigenvalues of the matrix pair (A, B) .
-

In practical applications, it is necessary to set some termination conditions for the optimization loop. Therefore, an error threshold ε is set as the stopping criterion

for the optimization process, i.e.,

$$\mathcal{L}(\boldsymbol{\theta}, \boldsymbol{\phi}) < \varepsilon.$$

Once the termination condition is met, the generalized eigenvalues of (A, B) are estimated by the ratios $\frac{t_{ii}}{s_{ii}}$ ($i = 1, \dots, N$ and $s_{ii} \neq 0$), where both real and imaginary parts of t_{ii} and s_{ii} are obtained through Hadamard test. The pseudo-algorithm is included in Algorithm 1.

θ_i and ϕ_i are the components of $\boldsymbol{\theta}$ and $\boldsymbol{\phi}$. To compute the partial derivatives of function $\mathcal{L}(\boldsymbol{\theta}, \boldsymbol{\phi})$ with respect to θ_i and ϕ_i , The Finite-difference approximation can be utilized [30]. This method is a numerical technique used to estimate the local rate of change of a function at a particular point. The partial derivatives can be specifically calculated using the following equations:

$$\begin{aligned} \frac{\partial \mathcal{L}(\boldsymbol{\theta}, \boldsymbol{\phi})}{\partial \theta_i} &= \frac{\mathcal{L}(\boldsymbol{\theta} + \Delta\theta_i \mathbf{u}_i, \boldsymbol{\phi}) - \mathcal{L}(\boldsymbol{\theta} - \Delta\theta_i \mathbf{u}_i, \boldsymbol{\phi})}{2\Delta\theta_i} \\ \frac{\partial \mathcal{L}(\boldsymbol{\theta}, \boldsymbol{\phi})}{\partial \phi_i} &= \frac{\mathcal{L}(\boldsymbol{\theta}, \boldsymbol{\phi} + \Delta\phi_i \mathbf{v}_i) - \mathcal{L}(\boldsymbol{\theta}, \boldsymbol{\phi} - \Delta\phi_i \mathbf{v}_i)}{2\Delta\phi_i} \end{aligned} \quad (6)$$

where $\Delta\theta_i$ and $\Delta\phi_i$ represent perturbations applied to $\boldsymbol{\theta}$ and $\boldsymbol{\phi}$, respectively. The vectors \mathbf{u}_i and \mathbf{v}_i are computational basis vectors with the same dimensions as $\boldsymbol{\theta}$ and $\boldsymbol{\phi}$, respectively. Typically, we set $\Delta\theta_i$ and $\Delta\phi_j$ to sufficiently small value.

V. COMPLEXITY ANALYSIS

In this section, we present the computation complexity analysis, which includes (1) Gate complexity: The total number of basic quantum gates (single and two qubit gates); (2) Qubit complexity: The total number of qubits required for the computation.

Theorem 3. Concerning the computational complexity of evaluating the loss function, the gate complexity is $O(n + 2^m \text{poly}(n))$. The qubit complexity is counted as $O(2n + m + 1)$.

Proof. The QPS technique requires only $O(n)$ gates in the variational quantum algorithm. For non-unitary matrices A and B , their implementation via LCU necessitates decomposition into 2^m unitary terms, contributing $O(2^m \text{poly}(n))$ gates. Additionally, the ansatz circuits $Q^\dagger(\boldsymbol{\theta})$ and $Z(\boldsymbol{\phi})$ each require $O(n)$ gates. The total gate complexity of the quantum circuit is $O(n + 2^m \text{poly}(n))$.

As shown in Fig. 1, the work register contains n work qubits, the index register contains 1 qubit, the ancilla register contains m qubit, and the augmented register contains n qubits. Thus the total qubit complexity is $O(2n + m + 1)$. \square

Compared to the classical generalized Schur decomposition with $O(2^{3n})$ computational complexity, when matrices A and B can be expressed as linear combinations of a small number of unitary matrices under the condition $n \gg m$ (e.g., for structured matrices like sparse or k -local Hamiltonians), the VQGE algorithm can demonstrate exponential quantum advantage. Otherwise, the

quantum advantage reduces to a linear level. Therefore, in practice, minimizing the number of unitary operators in the decomposition of A and B is critical for optimal performance.

VI. NUMERICAL RESULTS

A. Two-qubit system

We simulate the VQGE using randomly generated non-Hermitian matrices on the OriginQ cloud platform with QPanda [31]. The results confirm the feasibility of our proposed algorithm.

Example 1: Firstly, consider the randomly generated 2-qubit matrix pair (A, B) , where

$$A = \begin{pmatrix} -0.846053 & -3.121318 & 1.130982 & -0.135525 \\ -0.274860 & 0.540084 & 0.832479 & 0.530499 \\ -0.135770 & 0.613640 & 0.947157 & -0.638468 \\ 1.730607 & -1.242851 & -2.299600 & 0.060833 \end{pmatrix},$$

$$B = \begin{pmatrix} 0.217329 & 0.418199 & 1.206862 & 1.458747 \\ -0.208682 & -1.124809 & 0.288132 & 2.032686 \\ 1.272089 & -0.145261 & 1.799622 & 1.183555 \\ 0.000000 & 0.000000 & 0.000000 & 0.000000 \end{pmatrix}.$$

As shown in Fig. 2, the loss function converges to the order of 10^{-7} after approximately 900 iterations. The parameters $\boldsymbol{\theta}$ and $\boldsymbol{\phi}$ used at the 900th iteration are denoted as $\boldsymbol{\theta}_{opt}$ and $\boldsymbol{\phi}_{opt}$, respectively. The results show that the proposed method successfully find the generalized eigenvalues of (A, B) , and these eigenvalues can be estimated using the diagonal elements of matrices T and S .

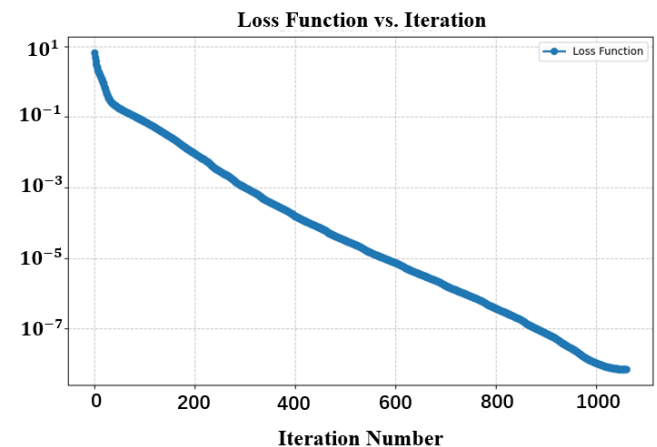


FIG. 2: The iterative process for computing the generalized eigenvalues of Example 1.

B. Application in ocean acoustic fields

Ocean acoustics is fundamental for investigating underwater sound propagation characteristics. The acous-

tic field solution can be formulated through the following differential equation system

$$\frac{d^2\varphi_m(z)}{dz^2} + \left(\frac{\omega^2}{c^2(z)} - k_m^2 \right) \varphi_m(z) = \mathbf{0},$$

$$\begin{cases} \frac{d\xi_{m,1}(z)}{dz} = -\xi_{m,2}(z) + \frac{1}{\mu(z)}\xi_{m,4}(z), \\ \frac{d\xi_{m,2}(z)}{dz} = \frac{\lambda(z)k_m^2}{\lambda(z) + 2\mu(z)}\xi_{m,1}(z) + \frac{1}{\lambda(z) + 2\mu(z)}\xi_{m,4}(z), \\ \frac{d\xi_{m,3}(z)}{dz} = \left(\frac{4\mu(z)(\lambda(z) + \mu(z))k_m^2}{\lambda(z) + 2\mu(z)} - \rho(z)\omega^2 \right) \xi_{m,1}(z) \\ \quad - \frac{\lambda(z)}{\lambda(z) + 2\mu(z)}\xi_{m,4}(z), \\ \frac{d\xi_{m,4}(z)}{dz} = -\rho(z)\omega^2\xi_{m,2}(z) + k_m^2\xi_{m,3}(z). \end{cases}$$

These equations describe the sound pressure mode propagation $\varphi_m(z)$ in seawater and the stress-displacement mode propagation $\xi_m(z) = (\xi_{m,1}(z), \xi_{m,2}(z), \xi_{m,3}(z), \xi_{m,4}(z))^T$ in ice layers, with the wave numbers k_m being unknowns. Through finite difference method, the system is converted into a generalized eigenvalue problem [26, 32, 33]

$$AV = BV\Sigma, \quad (7)$$

where A and B are 32×32 non-Hermitian sparse matrices, Σ is a diagonal matrix with generalized eigenvalues on its diagonal, and V is a matrix whose column vectors are the corresponding generalized eigenvectors. The specific forms of matrices A and B are given in [34]. Due to the singularity of matrix B , we employ a projection method to map B onto its non-singular subspace for enhanced algorithmic efficiency [24]. The generalized eigenvalues of the projected matrices remain highly consistent with those of the original matrices. Fig. 3 shows the iterative convergence of the corresponding loss function, reaching stable convergence after 50 iterations. We therefore select θ and ϕ obtained after the 50th iteration as θ_{opt} and ϕ_{opt} , which successfully yield the target generalized eigenvalues.

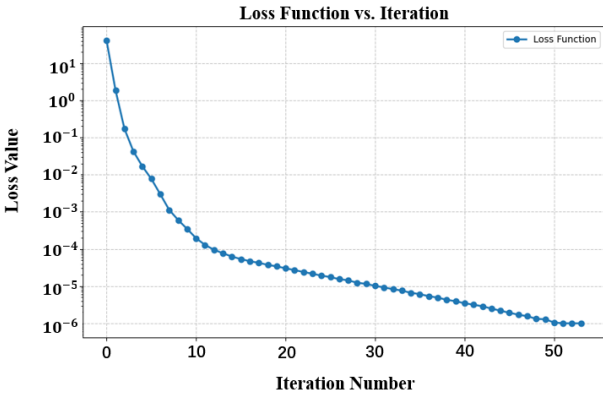


FIG. 3: The iterative process for computing the generalized eigenvalues in ocean acoustic fields.

C. Noise-incorporated simulation

Quantum noise presents a major challenge for implementing quantum algorithms on quantum virtual machines. To properly evaluate and optimize quantum algorithm performance, noise effects must be fully accounted for in numerical simulations. To this end, we introduce multiple configurable noise models that make the simulation environment more representative of real quantum computers. These models support fine-grained control over qubit states, quantum gate operations, and error parameters, enabling adaptation to noise environments of varying complexity.

The amplitude damping error models the qubit relaxation process in quantum systems. In our numerical simulations, this noise channel is implemented after each single-qubit gate operation through the Kraus operator representation:

$$\varepsilon_{AD}(\rho) = E_0\rho E_0^\dagger + E_1\rho E_1^\dagger$$

where $E_0 = \begin{pmatrix} 1 & 0 \\ 0 & \sqrt{1-\gamma} \end{pmatrix}$ and $E_1 = \begin{pmatrix} 0 & \sqrt{\gamma} \\ 0 & 0 \end{pmatrix}$ are the damping operators with rate parameter γ .

The Pauli-X error, a predominant model for bit-flip noise in quantum computing, describes the unintended transitions between the ground state $|0\rangle$ and excited state $|1\rangle$. In our numerical simulations, this noise channel is applied to the target qubit after each single-qubit gate operation with probability parameter p_1 , expressed as:

$$\varepsilon_X(\rho) = (1-p_1)\rho + p_1X\rho X^\dagger$$

where X denotes the Pauli operator.

The two-qubit depolarizing noise characterizes the quantum information randomization during controlled gate operations. When implementing two-qubit gates (e.g., CNOT or CZ), the system may degenerate into the maximally mixed state with probability p_2 due to gate imperfections. In our numerical simulations, we implement this noise channel after each two-qubit gate operation as:

$$\varepsilon_{depol}^{(2)}(\rho) = (1-p_2)\rho + \frac{p_2}{15} \sum_{(P_i, P_j) \neq (I, I)} (P_i \otimes P_j)\rho(P_i \otimes P_j)^\dagger$$

where $P_i \in \{I, X, Y, Z\}$ denotes Pauli operators, with the summation covering all non-identity two-qubit Pauli terms.

Example 2: Let $\gamma = 0.01$, $p_1 = 0.1$, and $p_2 = 0.3$. We randomly generate a 2-qubit matrix pair (A, B) , with the convergence process of the corresponding loss function shown in Fig. 4. The loss function exhibits a steady decreasing trend with iterations. Specifically:

(1) After approximately 6000 iterations, the loss value reaches below 10^{-6} ;

(2) The value further drops below 10^{-7} after around 8000 iterations.

When the error threshold is set to $\varepsilon < 10^{-6}$, θ and ϕ from the 6000th iteration can be selected as θ_{opt} and

ϕ_{opt} . These results demonstrate the algorithm's robustness under noisy conditions.

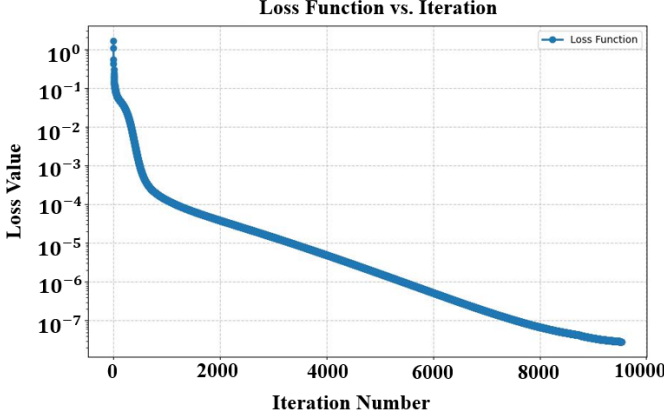


FIG. 4: The iterative process for computing the generalized eigenvalues of Example 2.

VII. CONCLUSION

In conclusion, we propose a variational quantum algorithm for generalized eigenvalues in non-Hermitian systems using generalized Schur decomposition, while designing a new loss function and demonstrating how to compute both the loss function and its gradients on near-term quantum devices. Finally, we validate the algorithm's performance through numerical simulations and demonstrate its application to generalized eigenvalue problems in ocean acoustics. Additional noise simulations confirm the algorithm's robustness. Overall, our work demonstrates the feasibility of computing generalized eigenvalues for non-Hermitian systems on near-term quantum devices.

ACKNOWLEDGEMENTS

This work is supported by the Stable Supporting Fund of Acoustic Science and Technology Laboratory (JCKYS2024604SSJS001), and the Fundamental Research Funds for the Central Universities (3072024XX2401).

Appendix A: Quantum process snapshot

In [14], the QPS technique measures all squared moduli $\{|\langle i|U|j\rangle|^2 | i, j = 0, 1, \dots, 2^n - 1\}$ of a $2^n \times 2^n$ unitary matrix U using the circuit shown in Fig. 5. We use CNOT^n to denote n CNOT gates with the control qubits in the work register and the target qubits in the augmented register, establishing a qubit-by-qubit correspondence. The

quantum circuit evolves the initial state $|0\rangle_w^{\otimes n} |0\rangle_{\text{aug}}^{\otimes n}$ into

$$\begin{aligned} & |0\rangle_w^{\otimes n} |0\rangle_{\text{aug}}^{\otimes n} \\ & \xrightarrow{H^{\otimes n} \otimes I^{\otimes n}} \frac{1}{\sqrt{2^n}} \sum_{i=0}^{2^n-1} |i\rangle_w |0\rangle_{\text{aug}}^{\otimes n} \\ & \xrightarrow{n \text{ CNOT}} \frac{1}{\sqrt{2^n}} \sum_{i=0}^{2^n-1} |i\rangle_w |i\rangle_{\text{aug}} \\ & \xrightarrow{I^{\otimes n} \otimes U} \frac{1}{\sqrt{2^n}} \sum_{i=0}^{2^n-1} |i\rangle_w U |i\rangle_{\text{aug}}. \end{aligned} \quad (\text{A1})$$

Thus, the $|\langle i|U|j\rangle|^2$ corresponds to the probability of obtaining the measurement outcome $|i\rangle_w |j\rangle_{\text{aug}}$.

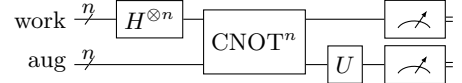


FIG. 5: Quantum circuit of QPS in [14].

Following this approach, measuring l unitary matrices would require l independent circuits. By introducing idx register with $\lceil \log l \rceil$ qubits, we extend this scheme to enable measurement of all l unitary matrices with just a single circuit. As shown in Fig. 6, the Hamiltonian selection oracle is defined as

$$\text{SELECT} = \sum_{i=0}^{l-1} |i\rangle \langle i| \otimes U_i.$$

The quantum circuit evolves the initial state $|0\rangle_w^{\otimes n} |0\rangle_a^{\otimes \lceil \log l \rceil} |0\rangle_{\text{aug}}^{\otimes n}$ into

$$\begin{aligned} & |0\rangle_w^{\otimes n} |0\rangle_a^{\otimes \lceil \log l \rceil} |0\rangle_{\text{aug}}^{\otimes n} \\ & \xrightarrow{H^{\otimes n} \otimes H^{\lceil \log l \rceil} \otimes I^{\otimes n}} \frac{1}{\sqrt{2^{n+\lceil \log l \rceil}}} \sum_{i=0}^{2^n-1} \sum_{j=0}^{2^{\lceil \log l \rceil}-1} |i\rangle_w |j\rangle_a |0\rangle_{\text{aug}}^{\otimes n} \\ & \xrightarrow{n \text{ CNOT}} \frac{1}{\sqrt{2^{n+\lceil \log l \rceil}}} \sum_{i=0}^{2^n-1} \sum_{j=0}^{2^{\lceil \log l \rceil}-1} |i\rangle_w |j\rangle_a |i\rangle_{\text{aug}} \\ & \xrightarrow{\text{SELECT}} \frac{1}{\sqrt{2^{n+\lceil \log l \rceil}}} \sum_{i=0}^{2^n-1} \sum_{j=0}^{2^{\lceil \log l \rceil}-1} |i\rangle_w |j\rangle_a U_j |i\rangle_{\text{aug}}. \end{aligned} \quad (\text{A2})$$

Thus, for any $0 \leq k \leq l-1$, the $|\langle i|U_k|j\rangle|^2$ equals the probability of obtaining the measurement outcome $|i\rangle_w |k\rangle_a |j\rangle_{\text{aug}}$.

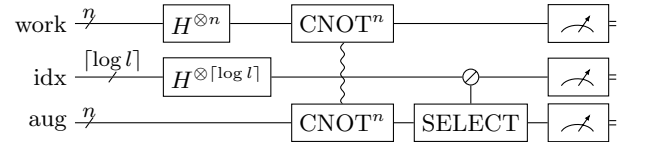


FIG. 6: Quantum circuit of QPS for multiple unitary matrices.

To compare the QPS circuits in Fig. 5 and Fig. 6, we performed numerical simulations with randomly generated unitary matrices (two 4×4 unitary matrices and four 8×8 unitary matrices). Fig. 7 and Fig. 8 show the relationship between the number of shots and the root mean squared error for both circuit designs. The results demonstrate that the circuit structure in Fig. 6 maintains measurement accuracy and error ranges comparable to the Fig. 5. For operational convenience, we adopt the scheme presented in Fig. 6 in this study.

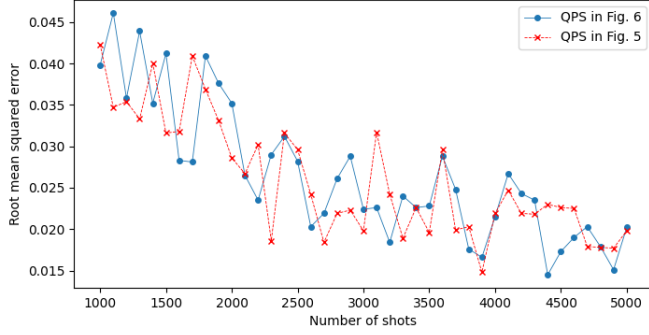


FIG. 7: Experimental results of QPS for two 4×4 unitary matrices.

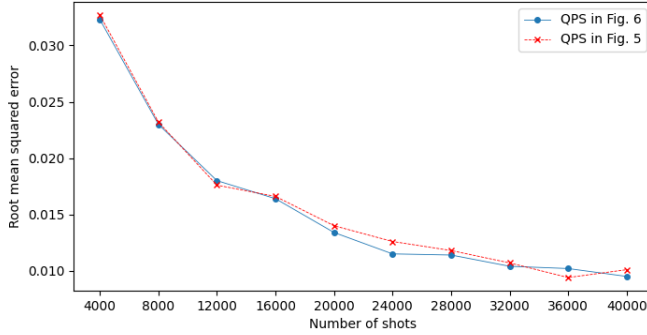


FIG. 8: Experimental results of QPS for four 8×8 unitary matrices.

Appendix B: Data input model based on LCU

Taking matrix A as an example. The LCU method needs to decompose a non-unitary matrix A into a linear combination of unitary matrices

$$A = \sum_{i=0}^{2^m-1} \alpha_i A_i, \quad (\text{B1})$$

where A_i are unitaries and $\alpha_i \in \mathbb{C}$. Fig. 9 demonstrates the corresponding quantum circuit implementation, employing state preparation oracles PREP and UNPREP to generate the quantum state

$$\begin{aligned} \text{PREP } |0\rangle^{\otimes m} &= \text{UNPREP}^\dagger |0\rangle^{\otimes m} \\ &= \frac{1}{\sqrt{c}} \sum_i \sqrt{\alpha_i} |i\rangle, \end{aligned}$$

where the normalization constant $c = \sum_{i=0}^{2^m-1} |\alpha_i|$, and the Hamiltonian selection oracle $\text{SELECT}(A)$ defined as

$$\text{SELECT}(A) = \sum_{i=0}^{2^m-1} |i\rangle \langle i| \otimes A_i.$$

which applies the unitary A_i conditioned on the state $|i\rangle$.

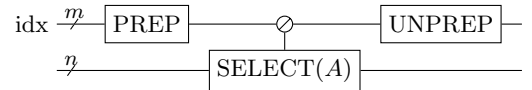


FIG. 9: Quantum circuit of LCU [35].

Appendix C: State evolution process in eq. (4)

When the idx register collapse to $|0\rangle^{\otimes \lceil \log m \rceil}$, the quantum circuit in Fig. 1 evolves the initial state $|0\rangle_w^{\otimes n} |0\rangle_a |0\rangle_{\text{aug}}^{\otimes n}$ into

$$\begin{aligned} &|0\rangle_w^{\otimes n} |0\rangle_a |0\rangle_{\text{aug}}^{\otimes n} \\ \xrightarrow{H^{\otimes n} \otimes H \otimes I^{\otimes n}} & \frac{1}{\sqrt{2^{n+1}}} \sum_{i=0}^{2^n-1} \left(|i\rangle_w |0\rangle_a |0\rangle_{\text{aug}}^{\otimes n} + |i\rangle_w |1\rangle_a |0\rangle_{\text{aug}}^{\otimes n} \right) \\ \xrightarrow{n \text{ CNOT}} & \frac{1}{\sqrt{2^{n+1}}} \sum_{i=0}^{2^n-1} \left(|i\rangle_w |0\rangle_a |i\rangle_{\text{aug}} + |i\rangle_w |1\rangle_a |i\rangle_{\text{aug}} \right) \end{aligned}$$

$$\begin{aligned}
& \xrightarrow{I^{\otimes n} \otimes I \otimes Z(\phi)} \frac{1}{\sqrt{2^{n+1}}} \sum_{i=0}^{2^n-1} \left(|i\rangle_w |0\rangle_a Z(\phi) |i\rangle_{\text{aug}} + |i\rangle_w |1\rangle_a Z(\phi) |i\rangle_{\text{aug}} \right) \\
& \xrightarrow{I^{\otimes n} \otimes (|0\rangle\langle 0| \otimes A + |1\rangle\langle 1| \otimes B)} \frac{1}{\sqrt{2^{n+1}}} \sum_{i=0}^{2^n-1} \left(|i\rangle_w |0\rangle_a AZ(\phi) |i\rangle_{\text{aug}} + |i\rangle_w |1\rangle_a BZ(\phi) |i\rangle_{\text{aug}} \right) \\
& \xrightarrow{I^{\otimes n} \otimes I \otimes Q^\dagger(\theta)} \frac{1}{\sqrt{2^{n+1}}} \sum_{i=0}^{2^n-1} \left(|i\rangle_w |0\rangle_a Q^\dagger(\theta) AZ(\phi) |i\rangle_{\text{aug}} + |i\rangle_w |1\rangle_a Q^\dagger(\theta) BZ(\phi) |i\rangle_{\text{aug}} \right) \\
& = \frac{1}{\sqrt{2^{n+1}}} \sum_{i=0}^{2^n-1} \left(|i\rangle_w |0\rangle_a T(\theta, \phi) |i\rangle_{\text{aug}} + |i\rangle_w |1\rangle_a S(\theta, \phi) |i\rangle_{\text{aug}} \right)
\end{aligned}$$

Appendix D: Design of parameterized circuits

This section presents several parameterized quantum circuit architectures implemented as unitary operators $Q^\dagger(\theta)$ and $Z(\phi)$. The architectures are demonstrated using 5-qubit systems for clarity, and all designs maintain scalability for larger quantum processors. Fig. 10 illustrates four quantum circuit ansatz architectures: (a) The basic hardware-efficient ansatz, employing fundamental combinations of single-qubit rotation gates and CNOT gates, forms the core architecture in quantum circuit design; (b) The dressed CNOT ansatz enhances controllability by incorporating rotation gates before and after each CNOT gate; (c) The cyclic entanglement ansatz, which introduces extra CNOT gates to form a closed-loop topology, theoretically improving entanglement capability; (d) The CNOT-effect-specific ansatz employs particular CNOT gate arrangements to systematically investigate their influence on quantum state evolution. When A and B contain only real elements, we take $U = R_y(\theta_i)$ to reduce the trainable parameters. Otherwise, we choose $U = R_z(\theta_{i_1})R_y(\theta_{i_2})R_z(\theta_{i_3})$ as a general rotation on the Bloch sphere to enhance expressibility. These ansatzes can be implemented with varying layers, and additional optimized architectures can be selected based on the characteristics of matrices A and B .

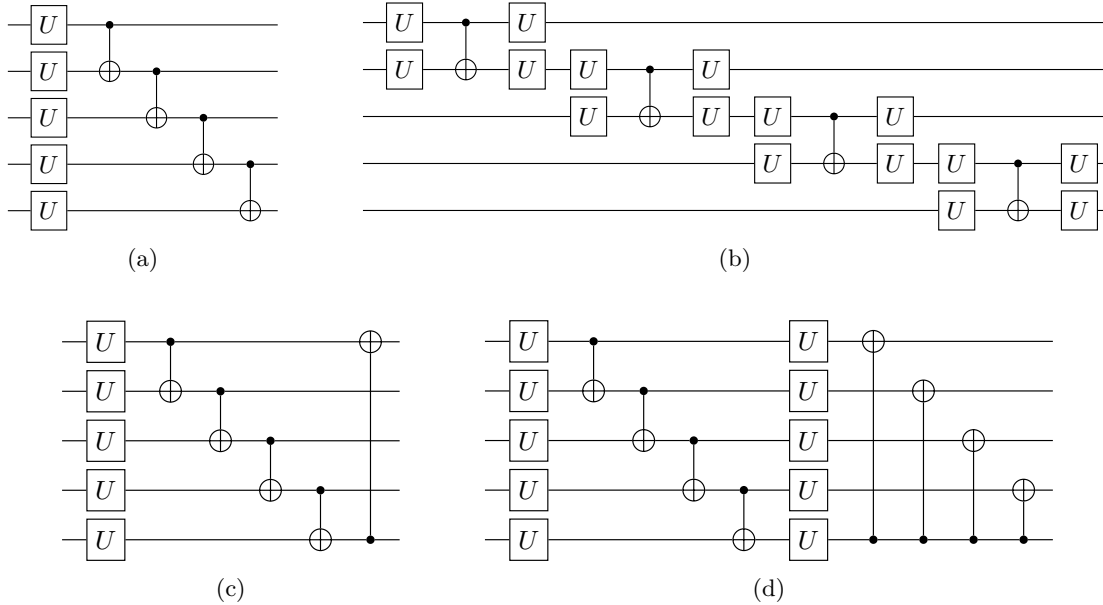


FIG. 10: Ansatz candidates considered in numerical experiments.

[1] M. R. Hestenes and W. Karush, A method of gradients for the calculation of the characteristic roots and vectors

of a real symmetric matrix, J. Res. Nat. Bur. Stand. **47**,

- 45 (1951).
- [2] W. W. Bradbury and R. Fletcher, New iterative methods for solution of the eigenproblem, *Num. Math.* **9**, 259 (1966).
- [3] E. Vecharynski, C. Yang, and J. E. Pask, A projected preconditioned conjugate gradient algorithm for computing many extreme eigenpairs of a hermitian matrix, *J. Comput. Phys.* **290**, 73 (2015).
- [4] F. Barahona, On the computational complexity of ising spin glass models, *J. Phys. A* **15**, 3241 (1982).
- [5] S. Wiesner, Simulations of many-body quantum systems by a quantum computer, arXiv: quant-ph/9603028 (1996).
- [6] D. Poulin and P. Wocjan, Preparing ground states of quantum many-body systems on a quantum computer, *Phys. Rev. Lett.* **102**, 130503 (2009).
- [7] D. S. Abrams and S. Lloyd, Simulation of many-body fermi systems on a universal quantum computer, *Phys. Rev. Lett.* **79**, 2586 (1997).
- [8] A. Smith, M. Kim, F. Pollmann, and J. Knolle, Simulating quantum many-body dynamics on a current digital quantum computer, *npj Quantum Inf.* **5**, 106 (2019).
- [9] A. Aspuru-Guzik, A. D. Dutoi, P. J. Love, and M. Head-Gordon, Simulated quantum computation of molecular energies, *Science* **309**, 1704 (2005).
- [10] P. J. O'Malley, R. Babbush, I. D. Kivlichan, J. Romero, J. R. McClean, R. Barends, J. Kelly, P. Roushan, A. Tranter, and N. Ding, Scalable quantum simulation of molecular energies, *Phys. Rev. X* **6**, 031007 (2016).
- [11] J. B. Parker and I. Joseph, Quantum phase estimation for a class of generalized eigenvalue problems, *Phys. Rev. A* **102**, 022422 (2020).
- [12] G. Raichel-Mieldzióć, S. Pliś, and E. Zak, Quantum algorithm for solving generalized eigenvalue problems with application to the schrödinger equation, arXiv: quant-ph/2506.13534v1 (2025).
- [13] A. Peruzzo, J. Clean, P. Shadbolt, M. H. Yung, X. Q. Zhou, P. J. Love, A. Aspuru-Guzik, and J. L. O'Brien, A variational eigenvalue solver on a photonic quantum processor, *Nat. Commun* **5**, 4213 (2014).
- [14] H. F. Zhao, P. Zhang, and T. C. Wei, A universal variational quantum eigensolver for non-hermitian systems, *Sci. Rep.* **13**, 22313 (2023).
- [15] X. D. Xie, Z. Y. Xue, and D. B. Zhang, Variational quantum algorithms for scanning the complex spectrum of non-hermitian systems, *Front. Phys.* **19**, 41202 (2024).
- [16] J. M. Liang, S. Q. Shen, M. Li, and S. M. Fei, Quantum algorithms for the generalized eigenvalue problem, *Quantum Inf. Process.* **21**, 23 (2022).
- [17] Y. Sato, H. C. Watanabe, R. Raymond, R. Kondo, K. Wada, K. Endo, M. Sugawara, and N. Yamamoto, Variational quantum algorithm for generalized eigenvalue problems and its application to the finite-element method, *Phys. Rev. A* **108**, 022429 (2023).
- [18] M. R. Hwang, E. Jung, M. Kim, and D. Park, Euclidean time method in generalized eigenvalue equation, *Quantum Inf. Process.* **23**, 62 (2024).
- [19] M. Cerezo, A. Arrasmith, R. Babbush, S. C. Benjamin, S. Endo, K. Fujii, J. R. McClean, K. Mitarai, X. Yuan, and L. Cincio, Variational quantum algorithms, *Nat. Rev. Phys.* **3**, 625 (2021).
- [20] A. Kandala, A. Mezzacapo, K. Temme, M. Takita, M. Brink, J. M. Chow, and J. M. Gambetta, Hardware-efficient variational quantum eigensolver for small molecules and quantum magnets, *Nature* **549**, 242 (2017).
- [21] O. Higgott, D. Wang, and S. Brierley, Variational quantum computation of excited states, *Quantum* **3**, 156 (2019).
- [22] H. L. Liu, Y. S. Wu, L. C. Wan, S. J. Pan, S. J. Qin, F. Gao, and Q. Y. Wen, Variational quantum algorithm for the poisson equation, *Phys. Rev. A* **104**, 022418 (2021).
- [23] X. Wang, Z. X. Song, and Y. L. Wang, Variational quantum singular value decomposition, *Quantum* **5**, 483 (2021).
- [24] G. H. Golub and C. F. V. Loan, *Matrix Computations*, 4th ed. (Johns Hopkins University Press, Baltimore, 2013).
- [25] A. Gilyén, Y. Su, G. H. Low, and N. Wiebe, Quantum singular value transformation and beyond: exponential improvements for quantum matrix arithmetics, in *Proc. 51st Annual ACM SIGACT Symposium on Theory of Computing* (Phoenix, AZ, USA, 2019) pp. 193–204.
- [26] C. L. Yang, Z. X. Li, H. M. Yao, Z. B. Fan, G. F. Zhang, and J. S. Liu, Dictionary-based sparse block encoding with low subnormalization and circuit depth, arXiv: quant-ph/2405.18007v2 (2024).
- [27] G. L. Long, General quantum interference principle and duality computer, *C. Theor. Phys.* **45**, 825 (2006).
- [28] A. M. Childs and N. Wiebe, Hamiltonian simulation using linear combinations of unitary operations, *Quant. Inf. Comput.* **12**, 901 (2012).
- [29] M. Cerezo, K. Sharma, A. Arrasmith, and P. J. Coles, Variational quantum state eigensolver, *npj Quantum Inf.* **8**, 113 (2022).
- [30] J. Nocedal and S. J. Wright, *Numerical Optimization* (Springer, New York, 2006).
- [31] OriginQ, Pyqpanda, <https://qcloud.originqc.com.cn>.
- [32] F. B. Jensen, W. A. Kuperman, M. B. Porter, H. Schmidt, and A. Tolstoy, *Computational Ocean Acoustics* (Springer New York, 2011).
- [33] K. Aki and P. G. Richards, *Quantitative Seismology*, 2nd ed. (University Science Books, 2002).
- [34] J. X. Li, Figshare, <https://doi.org/10.6084/m9.figshare.28815254>.
- [35] R. Babbush, C. Gidney, D. W. Berry, N. Wiebe, J. McClean, A. Paler, A. Fowler, and H. Neven, Encoding electronic spectra in quantum circuits with linear t complexity, *Phys. Rev. X* **8**, 041015 (2018).